

# Size and charge characterization of polymeric drug delivery systems by Taylor dispersion analysis and capillary electrophoresis

Amal Ibrahim · Rémi Meyrueix · Gauthier Pouliquen ·  
You Ping Chan · Hervé Cottet

Received: 15 January 2013 / Revised: 3 April 2013 / Accepted: 4 April 2013 / Published online: 28 April 2013  
© Springer-Verlag Berlin Heidelberg 2013

**Abstract** In this work, Taylor dispersion analysis and capillary electrophoresis were used to characterize the size and charge of polymeric drug delivery nanogels based on polyglutamate chains grafted with hydrophobic groups of vitamin E. The hydrophobic vitamin E groups self-associate in water to form small hydrophobic nanodomains that can incorporate small drugs or therapeutic proteins. Taylor dispersion analysis is well suited to determine the weight average hydrodynamic radius of nanomaterials and to get information on the size polydispersity of polymeric samples. The effective charge was determined either from electrophoretic mobility and hydrodynamic radius using electrophoretic modeling (three different approaches were compared), or by indirect UV detection in capillary electrophoresis. The influence of vitamin E hydrophobicity on the polymer effective charge has been studied. The presence of vitamin E leads to a drastic decrease in polymer effective charge in comparison to non-modified polyglutamate. Finally, the electrophoretic behavior of polyglutamate backbone grafted with hydrophobic vitamin E (pGVE) nanogels according to the ionic strength was investigated using the recently

proposed slope plot approach. It was deduced that the pGVE nanogels behave electrophoretically as polyelectrolytes which is in good agreement with the high water content of the nanogels.

**Keywords** Polymeric drug delivery system · Taylor dispersion analysis · Effective charge · Indirect UV detection · Slope plot · Ionic strength dependence of the electrophoretic mobility

## Introduction

There has been great interest in developing polymeric drug release systems that can maintain constant drug doses over long periods and tunable release of both hydrophilic and hydrophobic compounds [1–5]. Polymeric nanoparticles are emerging as an attractive treatment option for cancer due to their favorable size distribution, drug carrying capacity, tunable properties, and their ability to provide controlled release at a specific site [6–10]. Nanoscale hydrogels, or nanogels, with tunable chemical and physical properties, can be tailor-made to respond to environmental changes in order to ensure spatial and stimuli-controlled drug release in vivo [4, 11–13]. The characterization of nanogels remains a challenging issue due to the large number of physicochemical parameters and their distributions (e.g., molar mass, chemical composition, hydrophilic/hydrophobic balance, size, charge...) [14–16] that contribute to the system performances.

Biodegradable hydrogels consisting of hydrophilic polyglutamate backbone grafted with hydrophobic vitamin E, denoted pGVE, were developed by Flamel Technologies (Medusa® platform) [17]. The pGVE chains self-assemble in aqueous medium to form a stable solution of nano-sized

**Electronic supplementary material** The online version of this article (doi:10.1007/s00216-013-6972-4) contains supplementary material, which is available to authorized users.

A. Ibrahim · H. Cottet (✉)  
Institut des Biomolécules Max Mousseron (UMR 5247 CNRS-  
Université de Montpellier 1-Université de Montpellier 2), place  
Eugène Bataillon CC 1706,  
34095 Montpellier Cedex 5, France  
e-mail: hcottet@univ-montp2.fr

R. Meyrueix · G. Pouliquen · Y. P. Chan  
Flamel Technologies, Parc Club du Moulin à Vent, 33, avenue du  
Dr Georges Lévy,  
69693 Vénissieux, France

hydrogels comprising multiple polymer chains and 95 % water (see Fig. 1). The *in vivo* biodistribution of hydrogels is mainly governed by their size and the surface charge density. The main objective of this work was to characterize the size and the effective charge of pGVE hydrogels of different chain lengths with and without vitamin E modifications.

The size or the hydrodynamic radius ( $R_h$ ) is generally determined by dynamic light scattering (DLS), by DOSY NMR, or by SEC with multiple detection including a viscosimeter. More recently, Taylor dispersion analysis (TDA) has been used for different kinds of solutes including small molecules/ions and drugs [18, 19], polymers [20–22], nanoparticles [23], dendrimers [24], therapeutic peptides, proteins, and liposomes [25–29]. TDA presents several advantages such as: low injection volumes (approximately in nanoliter) [30], absolute determination without calibration from angstrom to submicron, and determination of the weight average  $R_h$  instead of harmonic  $z$ -average in the case of DLS [31]. In the case of bimodal size distribution, the deconvolution of the taylorgram allows determining the size and the relative proportion of the two populations constituting the sample [20].

Effective charge ( $q_{\text{eff}}$ ) is the real charge of a (macro)molecule, taking into account all the ionized groups and any ionic species tightly associated with it [32], which controls the electrostatic interactions with neighboring charged (macro)molecules [33].  $q_{\text{eff}}$  determination of polymeric systems is a challenging issue because it depends on several parameters such as pH (dissociation of ionized groups), counter ion condensation (Manning theory) [34], and on possible specific interactions such as hydrophobic effects [35, 36] and weak interactions [37]. Different methods were investigated for effective charge determination including conductivity measurements [38], osmotic pressure [39], light scattering techniques [40], and electrophoretic technique [32, 41–48]. Regarding electrophoretic methods, one can distinguish the approaches based on electrophoretic mobility measurement combined to electrophoretic modeling [48] from those basically relying on the Kohlrausch regulating function (KRF) and allowing a direct determination of the effective charge by indirect UV detection mode [42] or by isotachopheresis [43].

In this work, the characterization in size and effective charge of pGVE hydrogels was investigated using TDA and electrophoretic techniques.

## Theoretical background

### Taylor dispersion analysis

The concept of TDA was presented a long time ago by Taylor [49] and was later extended by Aris [50]. It is based on the dispersion of a solute plug in a laminar Poiseuille flow. This dispersion resulted from the combination of the dispersive velocity profile with the molecular diffusion that redistributes the molecules over the tube cross section. The band broadening resulting from Taylor dispersion can be easily quantified via the temporal variance ( $\sigma^2$ ) of the elution profile. The determination of the temporal variance is usually done by fitting the elution peak by a Gaussian fitting in the case of monodisperse samples or by integration of the peak in the case of polydisperse samples [24, 51]:

$$\sigma^2 = \frac{\int h_i(t - t_d)^2 dt}{\int h_i dt} \quad (1)$$

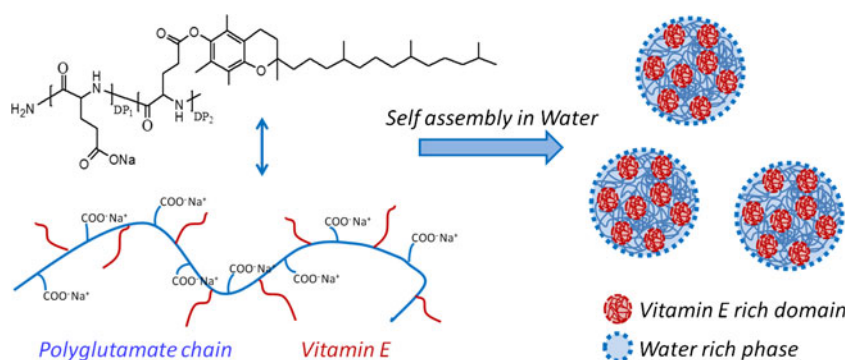
where  $h_i$  is the detector response (generally the UV absorbance vs time at a given detection point), and  $t_d$  is the elution time. The molecular diffusion coefficient ( $D$ ) and  $R_h$  values are then calculated by the following equations:

$$D = \frac{R_c^2 t_d}{24\sigma^2} \quad (2)$$

$$R_h = \frac{k_B T}{6\pi\eta D} = \frac{4\sigma^2 k_B T}{\pi\eta R_c^2 t_d} \quad (3)$$

where  $R_c$  is the capillary radius (in meter),  $k_B$  is the Boltzmann constant ( $1.38 \times 10^{-23} \text{ J K}^{-1}$ ),  $T$  is the absolute temperature (in kelvin), and  $\eta$  is the viscosity of the eluent. Equation 3 is valid when  $t_d$  is much longer than the characteristic diffusion time of the solute in the cross section of the

**Fig. 1** Chemical structure of pGVE chains and representation of the nanogels in water. Number of charged Glu monomers per polymer chain ( $DP_1$ ) and number of uncharged Glu-VE monomers per polymer chain ( $DP_2$ )



capillary (i.e.,  $t_d \geq 1.4 R_c^2/D$ ) and when the axial diffusion is negligible compared to convection (i.e., when the Peclet number  $Pe = R_c u/D$  is superior to 69 [23, 52], with  $u$  being the linear mobile phase velocity). TDA could be easily performed on a capillary electrophoresis apparatus with single or double detection points [53]. The latter is used to avoid corrections of the temporal variance and elution time from the pressure ramp time and the solute injected volume. However, when the volume of the injected plug is smaller than 1 % of the capillary volume to the detector, corrections are negligible. In this case, TDA with a single detection point leads to similar results compared to TDA with two detection points [53].

Effective charge determination

In this work, four methods of effective charge determination were applied and compared. A summary of these methods (input parameters and equations) is available as electronic supplementary material, Table S1.

Nernst–Einstein relationship

The first method is based on the Nernst–Einstein relationship (NE) [54, 55]:

$$z_{\text{eff}} = \frac{6\pi\eta R_h \mu_{\text{ep}}^\infty}{e} \tag{4}$$

where  $z_{\text{eff}}$  is the effective charge number of the solute, and  $\mu_{\text{ep}}^\infty$  is the limiting mobility (i.e., electrophoretic mobility at infinite dilution) which cannot be experimentally determined. Some theoretical models are available to extrapolate  $\mu_{\text{ep}}$  to zero ionic strength using the Pitts model [56, 57] for mono-charged small ions or the Friedl model [58] for multi-

charged small ions ( $z=2-6$ ). Up to date, there is no model available to extrapolate  $\mu_{\text{ep}}^\infty$  for polyelectrolytes or nanoparticles. As a consequence, applying the NE model at finite ionic strength, for which the electrophoretic retardation and relaxation effects cannot be neglected, leads to underestimated effective charge [47, 59]. Nevertheless, for a matter of comparison, we have decided to present the effective charge results given by this approach.

O’Brien–White–Ohshima model

A second method based on the O’Brien–White–Ohshima model (OWO) can be used for  $z_{\text{eff}}$  determination of (nano)particles with  $\kappa R_h \leq 10$  and zeta potential  $\zeta \leq 100$  mV ( $e\zeta/k_B T \leq 4$ ) in 1:1 electrolytes [60]:

$$\mu_{\text{ep}} = \frac{2\varepsilon_0\varepsilon_r\zeta}{3\eta} \left[ f_1(\kappa R_h) - \left(\frac{e\zeta}{k_B T}\right)^2 f_3(\kappa R_h) - \frac{m_- + m_+}{2} \left(\frac{e\zeta}{k_B T}\right)^2 f_4(\kappa R_h) \right] \tag{5}$$

where  $\varepsilon_r$  is the relative electric permittivity,  $\varepsilon_0$  is the electric permittivity of a vacuum, and  $e$  is the elementary electric charge, all in international units.  $\kappa$  is the Debye–Hückel parameter in  $\text{m}^{-1}$  ( $\kappa = 3.288 \times 10^9 \sqrt{I}$ ;  $I$  is the ionic strength in mole per liter), and  $f_1, f_3,$  and  $f_4$  are functions of  $\kappa R_h$  given in ref. [60].  $m_-$  and  $m_+$  are dimensionless ionic drag coefficients accessible by equations given in ref. [60]. The last analytical expression is used to plot  $\mu_{\text{ep}}$  as a function of  $\kappa R_h$  at different  $\zeta$ , which permits the graphical determination of  $\zeta$  from the experimental  $\mu_{\text{ep}}$  and  $R_h$  values at a given  $I$  (see electronic supplementary material, Fig. S1). Next, knowing  $\zeta$  and  $R_h$ , the surface charge density ( $\sigma$ ) is calculated by the following empirical equation derived by Ohshima et al. [61]:

$$\sigma = \frac{2\varepsilon_0\varepsilon_r\kappa k_B T}{ze} \sinh\left(\frac{ze\zeta}{2k_B T}\right) \left[ 1 + \frac{1}{\kappa R_h} \frac{2}{\cosh^2(ze\zeta/4k_B T)} + \frac{1}{(\kappa R_h)^2} \frac{8 \ln[\cosh(ze\zeta/4k_B T)]}{\sinh^2(ze\zeta/2k_B T)} \right]^{1/2} \tag{6}$$

Finally, from  $\sigma$  and  $R_h$ ,  $z_{\text{eff}}$  is calculated by:

$$z_{\text{eff}} = \frac{4\pi\sigma R_h^2}{e} \tag{7}$$

Modified Yoon and Kim model

The third theoretical model for  $z_{\text{eff}}$  determination of small weakly charged ellipsoids was first proposed by Yoon and Kim (YK) [62] and later extended by Allison et al. [63] to

take into account the relaxation effects. The latter model is applicable to nanoparticles of  $\kappa R_h \leq 25$  and  $\zeta \leq 200$  mV. In the framework of this model, the effective charge is directly related to electrophoretic mobility and hydrodynamic radius via Eq. 8:

$$z_{\text{eff}} = \frac{6\pi\eta R_h(1 + \kappa R_h)\mu_{\text{ep}}}{e g'(\kappa R_h) C(\kappa R_h, p)} \tag{8}$$

where  $g'(\kappa R_h)$  is the size correction function given to good approximation by [64]:

$$g'(\kappa R_h) \cong g(\kappa R_h) \cong 1 + \frac{1}{2 \left( 1 + \frac{5}{2\kappa R_h(1+2e^{-\kappa R_h})} \right)^3} \quad (8a)$$

and  $C(\kappa R_h, p)$  represents the relaxation correction calculated by the following:

$$C(\kappa R_h, p) = \frac{\mu(\text{relax})}{\mu(\text{no relax})} = 1 - \frac{\phi(\kappa R_h, p)p^2}{10} \quad (8b)$$

where:

$$p = 0.1 y_{\text{LPB}} = \frac{0.1 e^2 z'_{\text{eff}}}{4\pi \varepsilon_0 \varepsilon_r R_h (1 + \kappa R_h) k_B T} \quad (8c)$$

with  $y_{\text{LPB}}$  as the reduced (linear Poisson–Boltzmann) zeta potential.  $z'_{\text{eff}}$  is an estimation of the effective charge without accounting for the relaxation effects:

$$z'_{\text{eff}} = \frac{6\pi\eta R_h (1 + \kappa R_h) \mu_{\text{ep}}}{e g'(\kappa R_h)} \quad (8d)$$

The quantity  $\phi$  can be determined for any size spherical particle using the O'Brien and White procedure [65] by fitting  $\phi$  as a function of  $\kappa R_h$  and  $p$  in NaCl background electrolyte (BGE) at 298.15 K [63]:

$$\phi(\kappa R_h, p) = f_0(\kappa R_h) \exp\{-[f_1(\kappa R_h)p + f_2(\kappa R_h)p^2 + f_3(\kappa R_h)p^3 + f_4(\kappa R_h)p^4]\} \quad (8e)$$

$$f_0(x) = 48.91 (1 - e^{-1.08x}) \quad (8f)$$

$$f_1(x) = 0.037 \quad (8g)$$

$$f_2(x) = 3.023 + 1.189 \ln(x) - 0.118(\ln(x))^2 - 0.026(\ln(x))^3 \quad (8h)$$

$$f_3(x) = -0.033 \quad (8i)$$

$$f_4(x) = -1.749 - 1.058 \ln(x) + 0.006(\ln(x))^2 + 0.038(\ln(x))^3 \quad (8j)$$

This model is a straightforward method which does not require the extrapolation of  $\mu_{\text{ep}}^\infty$ , nor the determination of  $\zeta$  using graphical representation.

### Indirect UV detection mode

The fourth experimental approach proposed in this work is based on the indirect UV detection (IUV) in capillary electrophoresis (CE) [66–68] for the direct  $z_{\text{eff}}$  determination of polyelectrolytes [42, 48]. This detection mode consists in using a UV-absorbing chromophore (co-ion of the solute) which is displaced by the non-absorbing solute when applying the electric field in CE. This displacement leads to a negative peak due to a decrease in the background absorbance. The peak area is proportional to the quantity of the displaced chromophore, which in turn depends on the effective charge of the solute. This displacement is directly correlated to the KRF [69] which permits the calculation of the solute effective charge by the following equation:

$$z_{\text{eff}} = z_A \frac{\alpha_S}{\alpha_A} \times \frac{\mu_S (\mu_A + \mu_C)}{\mu_A (\mu_S + \mu_C)} \quad (9)$$

where  $z_{\text{eff}}$  and  $z_A$  are respectively the effective charge numbers of the solute and the chromophore.  $\mu_A$ ,  $\mu_S$ , and  $\mu_C$  are the absolute values of effective mobility of the chromophore, the solute, and the counter ion, respectively.  $\alpha_S$  is the slope of the calibration plot of the solute based on the time-corrected peak area (peak area normalized by its migration time) as a function of the solute molar concentration in indirect UV detection mode.  $\alpha_A$  is the slope of the calibration plot of the chromophore in direct UV detection at the same wavelength of detection used for the solute detection. The ratio  $\alpha_S/\alpha_A$  represents the transfer ratio defined as the number of moles of chromophore displaced by mole of solute.

In the case of a polymeric solute, it is convenient to introduce the effective charge number per charged monomer ( $z_1$ ) instead of the effective charge numbers of the solute entity ( $z_{\text{eff}}$ ).  $z_1$  is obtained by Eq. 9 when using the solute molar concentration in charged monomer ( $C_{M,1}$ ) to determine  $\alpha_S$ .

IUV method presents the advantage that it does not require any electrophoretic mobility modeling, and it is applicable to all kinds of solutes. It is based on the sensitivity of detection (i.e., on peak areas) instead of being essentially based on electrophoretic mobility (i.e., on migration times). Moreover, it has been demonstrated that this method was the only one among the four aforementioned ones to be applicable to (free-draining evenly charged) polyelectrolytes [48] which behave differently from (hard core surface-charged) nanoparticles. On the other hand, IUV method requires a suitable chromophore that does not interact with the solute and this method is limited to low ionic strengths.

**Materials and methods**

**Chemicals**

*p*-Anisic acid, bis(2-hydroxyethyl)amino-tris(hydroxymethyl)methane (BisTris), and hydroxypropyl cellulose (HPC,  $M_w=10^5 \text{ g mol}^{-1}$ ) were purchased from Sigma-Aldrich (Steinheim, Germany). Ammediol was from Avocado (Heysham, England). Glacial acetic acid was purchased from Carlo Erba (Paris, France). Hydrochloric acid, sodium chloride, and sodium hydroxide were from VWR (Leuven, Belgium). Deionized water was further purified with a Milli-Q system from Millipore (Molsheim, France).

**Samples**

Biodegradable pGVE hydrogels from Medusa<sup>®</sup> platform were developed by Flamel Technologies (Vénissieux, France). These drug delivery systems are administrated by subcutaneous injection, a depot is formed at the injection site, and the active drug/compound is slowly released in vivo over 1 to 14 days in humans. pGVE hydrogels are based on a hydrophilic biodegradable polyglutamate chain chemically derivatized with hydrophobic vitamin E. These formulations are statistical copolymers of negatively charged glutamate (Glu) and uncharged vitamin E-modified glutamate (Glu-VE) as shown in Fig. 1. The molar fraction of charged Glu monomers in the polymer chain is given by:

$$f = \frac{DP_1}{DP_1 + DP_2} \tag{10}$$

where  $DP_1$  is the number of underivatized charged Glu residues per polymer chain, and  $DP_2$  is the number of

Glu-VE monomers per polymer chain. The degree of polymerization of one polymer chain is thus:

$$DP = DP_1 + DP_2 \tag{11}$$

To determine  $z_1$  resulting from IUV method, the molar concentration in charged glutamate ( $C_{M,1}$ ) should be calculated according to:

$$C_{M,1} = \frac{C_{m,S}}{fM_1 + (1-f)M_2} \tag{12}$$

where  $C_{m,S}$  is the mass concentration of the polymeric solute, and  $M_1$  and  $M_2$  are the molar masses of the charged monomer (Glu) and uncharged monomer (Glu-VE), respectively.  $f$  is the molar fraction in charged Glu as defined by Eq. 10.

The hydrophobic vitamin E groups self-associate in water to form small hydrophobic nanodomains [17]. This results in the aggregation of  $N$  pGVE chains to form highly hydrated hydrogels of nanometric size (see Fig. 1). Table 1 gives the characteristics ( $DP$ s and  $N$  values given by the manufacturer) of the samples studied in this work. As for the notation, pGVE 50-20 means that the total number of monomers per polymer chain is 50 and the molar percentage of vitamin E is 20 % (i.e., ten VE-modified monomers per chain).

**Capillary coating**

Fused silica capillaries are coated using a 5 % (w/w) HPC solution prepared at room temperature and left overnight to eliminate bubbles. The capillaries (50  $\mu\text{m}$  i.d.) were filled with the polymer solution using a syringe pump at 0.03 mL/h. A stream of  $N_2$  gas at 3 bar was used to remove the excess HPC solution and was maintain during the immobilization process of the HPC performed by heating the

**Table 1** Physicochemical characteristics of the samples studied in this work

| Sample      | $DP$ | $DP_1$ | $DP_2$ | $N^a$ | $D^b$ | $R_h^c$ | RSD <sup>d</sup> | $\mu_S^e$ |
|-------------|------|--------|--------|-------|-------|---------|------------------|-----------|
| pGlu 50     | 50   | 50     | 0      | 1     | 9.14  | 2.7     | 1.3              | -35.0     |
| pGlu 220    | 220  | 220    | 0      | 1     | 4.01  | 6.1     | 2.2              | -33.5     |
| pGVE 50-20  | 50   | 40     | 10     | 10    | 5.67  | 4.3     | 2.1              | -36.4     |
| pGVE 100-20 | 100  | 80     | 20     | 4     | 6.02  | 4.1     | 2.1              | -36.0     |

$DP$  Total degree of polymerization of one polymer chain,  $DP_1$  number of charged monomers (Glu) per polymer chain,  $DP_2$  number of uncharged Glu-VE monomers per polymer chain,  $N$  number of chains per nanogel entity,  $D$  diffusion coefficient,  $R_h$  Hydrodynamic radius,  $\mu_S$  effective mobility

<sup>a</sup> Determined by static light scattering (data supplied by Flamel Technologies)

<sup>b</sup> Determined by TDA (in  $10^{-11} \text{ m}^2 \text{ s}^{-1}$ )

<sup>c</sup> Determined by TDA (in nanometer)

<sup>d</sup> RSD on  $R_h$  determination given in percent on  $n=3$  for each sample ( $n=6$  for pGVE 50-20)

<sup>e</sup> In  $10^{-9} \text{ m}^2 \text{ s}^{-1} \text{ V}^{-1}$  determined by CE in IUV mode (for experimental conditions, see Fig. 3). Temperature, 25 °C

capillary in a GC oven (GC-14A, Shimadzu, France). The temperature program was: 60 °C for 10 min followed by a temperature ramp from 60 to 140 °C at 5 °C/min and finally, 140 °C for 20 min. Before use, the coated capillaries were rinsed with water for 10 min.

#### Taylor dispersion analysis

TDA was performed on Agilent 3D-CE system (Walbronn, Germany) equipped with a diode array detector.  $R_h$  of all samples was determined in the following eluent: 50 mM BisTris/5 mM acetic acid, pH 7.4. Uncoated fused silica capillaries (Composite Metal Services, Worcester, UK) were used for pGVE samples, and the new capillaries were conditioned with the following flushes: 1 M NaOH for 30 min, 0.1 M NaOH for 30 min, and water for 5 min. For pGlu samples, HPC-coated capillaries were used (see “Capillary coating” section). Capillary dimensions were 33.5 cm total length (25 cm to the UV detector) × 50 μm i.d. Between runs, the capillary was flushed for 3 min with water then for 5 min with the eluent. All samples were diluted in the eluent (viscosity  $\eta=0.89 \cdot 10^{-3}$  Pa·s at 25 °C) and injected hydrodynamically (17 mbar, 5 s). In these conditions, the ratio of the injected volume to the capillary volume to the detector was lower than 1 % (0.9 %).  $t_d$  was corrected from the pressure ramp time by subtraction of  $t_{\text{ramp}}/2$  (~5 s).  $t_d$  and  $\sigma^2$  were also corrected for the finite length of the injection plug using Eqs. 11 and 12 reported in ref [24]. Mobilization pressure of 50 mbar was applied with eluent vials at both ends of the capillary. The temperature of the capillary cartridge was set at 25 °C. Taylorgrams were recorded at 200 nm for all samples.  $t_d$  was taken at the top of the taylorgrams, and  $\sigma^2$  was obtained by integration of the elution profile using Eq. 1 and Microsoft Excel software.  $R_h$  was calculated by Eq. 3. TDA conditions were verified and fulfilled.

#### Capillary electrophoresis

CE was carried out on Agilent 3D-CE instrument (Walbronn, Germany) equipped with a diode array detector. Uncoated fused silica capillaries (Composite Metal Services, Worcester, UK) of 50 cm total length (41.5 cm to the UV detector) × 50 μm i.d. were used for all samples. New capillaries were conditioned by flushing 1 M NaOH for 30 min, 0.1 M NaOH for 30 min, and finally water for 5 min. Between runs, the capillary was flushed with 1 M NaOH for 1 min, water for 1 min, then 3 min with the buffer. Samples were prepared in ultrapure water and injected hydrodynamically at the inlet end of the capillary (17 mbar, 10 s). The applied voltage was +20 kV, and the temperature of the capillary cartridge was set at 25 °C. A buffer composed of 50 mM BisTris/5 mM *p*-anisic acid (as

chromophore), pH 7.4, was used for the IUV analysis of pGlu and pGVE samples. For the calibration of *p*-anisic acid, a non-absorbing buffer composed of 50 mM BisTris/5 mM acetic acid was used. Data were collected at 245 nm. Electropherograms were plotted in electrophoretic mobility scale. Effective mobilities ( $\mu_{\text{ep}}$ ) of solutes were calculated using:

$$\mu_{\text{ep}} = \left( \frac{1}{t_m} - \frac{1}{t_{\text{eo}}} \right) \frac{LV}{V} \quad (13)$$

where  $\mu_{\text{ep}}$  is the effective mobility,  $l$  is the effective capillary length to the detection point,  $L$  is the total capillary length,  $V$  is the applied voltage,  $t_m$  is the migration time of the solute, and  $t_{\text{eo}}$  is the detection time of the electroosmotic flow (EOF).

## Results and discussion

The characteristics of the different pGVE copolymer samples from the Medusa platform studied in this work are described in Table 1, and a representation of the assembly of the copolymer into nanogels is depicted in Fig. 1. In this work, the characterization in size and charge of pGVE samples has been investigated. In particular, the influence of VE on the effective charge was studied taking non-modified pGlu chains of *DP* 50 and 220 for comparison.

#### Hydrodynamic radius determination by Taylor dispersion analysis

The size is an important characteristic parameter of nanogel drug delivery systems since it mainly controls the in vivo diffusion and biodistribution. Moreover, the  $R_h$  determination is required for the effective charge determination using NE, OWO, and YK modelings. TDA was performed using an eluent composed of 50 mM BisTris/5 mM acetic acid, pH 7.4 ( $I=5$  mM ionic strength). The experimental conditions of TDA are similar to those employed for effective charge determination by IUV (see “Effective charge determination” section). Figure 2 displays the taylorgrams obtained for all samples using a fused silica capillary for pGVE samples and an HPC-coated capillary for pGlu samples. Tailing peaks were obtained for pGlu samples when using a fused silica capillary (results not shown) explaining the choice of HPC-coated capillary for these samples. Symmetrical taylorgrams were obtained which is a good indication of the absence of capillary–solute interactions. Taylorgrams present non-Gaussian shape due to some size polydispersity.  $R_h$  was thus determined by integration of the entire elution profile using Eq. 1 to get  $\sigma^2$ .  $D$  and  $R_h$  were calculated via Eqs. 2 and 3, and average values on three repetitions are presented in

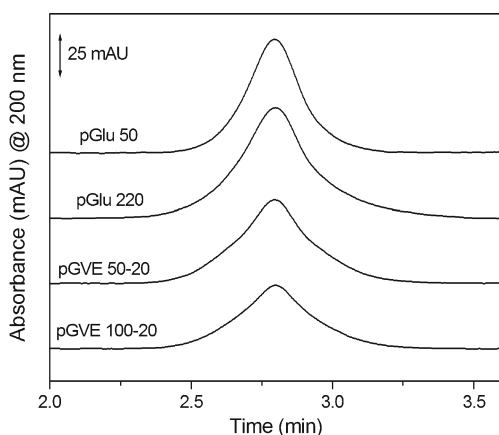


**Fig. 2** Taylorgrams of pGlu and pGVE samples having different  $DP$  and vitamin E percentages. Experimental conditions: fused silica capillary (HPC-coated capillary for pGlu 50 and pGlu 220 to avoid solute adsorption onto the capillary wall) of 33.5 cm total length (25 cm to the detector)  $\times$  50  $\mu\text{m}$  i.d. Eluent, 50 mM BisTris/5 mM acetic acid, pH 7.4. Mobilization pressure, 50 mbar. Hydrodynamic injection, 17 mbar, 5 s. Sample concentration, 2.5–3  $\text{g L}^{-1}$  in the eluent. Temperature, 25  $^{\circ}\text{C}$

Table 1. Assuming that the response of the UV detector is sensitive to the mass concentration in the polymer (peak area proportional to the mass concentration), the average  $R_h$  values determined by TDA are the weight average hydrodynamic radii [31] which are very different from the classical harmonic  $z$ -average value derived from DLS measurements. It can be noticed that all samples have nanometric radii ranging from 2.7 to 6.1 nm. For pGVE 50-20, the  $R_h$  (4.3 nm) was found higher than for pGlu 50 (2.7 nm). This can be explained by the high number ( $N=10$ ) of polymer chains in the polymeric assembly despite the

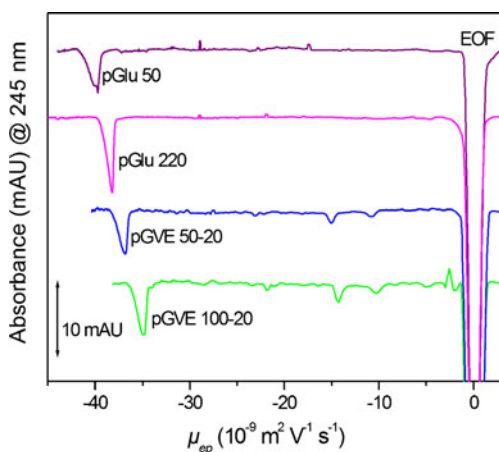


**Fig. 3** Electropherograms of pGlu ( $DP$  50 and 220) and of pGVE samples with different  $DP$  and vitamin E percentages obtained in IUV detection. Experimental conditions: fused silica capillary 50 cm (41.5 cm to the detector)  $\times$  50  $\mu\text{m}$  i.d. BGE, 50 mM BisTris/5 mM anisic acid, pH 7.4. Voltage, 20 kV. Hydrodynamic injection, 17 mbar, 10 s. Sample concentration, 0.5  $\text{g L}^{-1}$  for pGlu and 1.5  $\text{g L}^{-1}$  for pGVE. Temperature, 25  $^{\circ}\text{C}$

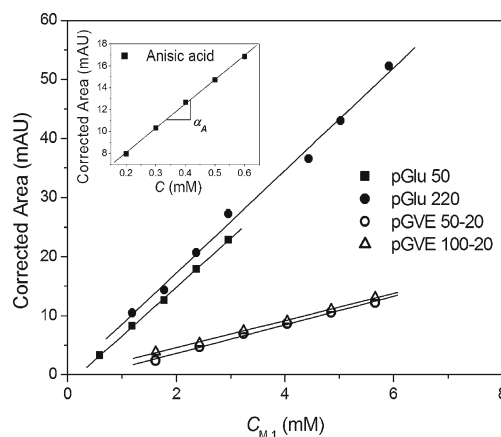


**Fig. 4** Calibration curves obtained by CE in indirect UV detection mode at 245 nm for pGlu and pGVE samples (*insert*: calibration curve for anisic acid—chromophore—in direct mode at 245 nm). Experimental conditions: fused silica capillary 50  $\mu\text{m}$  i.d.  $\times$  50 cm (41.5 cm to the detector). BGE, 50 mM BisTris/5 mM anisic acid, pH 7.4 (*insert*: 50 mM BisTris/5 mM acetic acid, pH 7.4). Voltage, 20 kV. Hydrodynamic injection, 17 mbar, 10 s. Temperature, 25  $^{\circ}\text{C}$

contraction effect due to the hydrophobicity of the VE groups. The relative standard deviations (RSD) on the  $R_h$  values are presented in Table 1, and are all lower than 2.2 % ( $n=3$  for all samples, except  $n=6$  for the pGVE 50-20 sample). TDA was found to be a simple, repeatable, and straightforward method for the determination of the weight average hydrodynamic radius.

#### Effective charge determination

IUV in CE was applied to samples presented in Table 1 using a BGE composed of 50 mM BisTris/5 mM *p*-anisic acid, pH 7.4. *p*-Anisic acid was chosen as a chromophore since it is a mono-charged anion (effective charge number,  $z_A=-1$ ) that is completely dissociated at pH 7.4 and that presents a strong molar extinction coefficient at 245 nm. At this wavelength, the samples have no UV absorbance. In addition, *p*-anisic acid has an effective mobility ( $\mu_{ep}=27.6 \cdot 10^{-9} \text{ m}^2 \text{ s}^{-1} \text{ V}^{-1}$  in this BGE) which is similar to the solute effective mobilities. This should help in having symmetrical peak by limiting the dispersion by electromigration. The displacement of the chromophore by the solute generates negative peaks as displayed in Fig. 3 at 245 nm. The sensitivity of detection of each sample was determined by calculating  $\alpha_S$ , the slope of the calibration curve obtained by plotting the time-corrected peak area as a function of the molar concentration in charged glutamate  $C_{M,1}$  calculated by Eq. 12 (see Fig. 4).

The sensitivity of detection of the chromophore  $\alpha_A$  was similarly determined by a calibration curve realized in direct UV mode at 245 nm using a transparent BGE composed of 50 mM BisTris/5 mM acetic acid, pH 7.4 (see the insert of Fig. 4). Using Eq. 9 (taking into consideration that  $C_{M,1}$  was

**Table 2** Effective charge numbers per nanogel entity ( $z_{\text{eff}}$ ) or per charged monomer (i.e., Glu residue,  $z_1$ ) using different electrophoretic approaches: Nernst–Einstein (NE), O’Brien–White–Ohshima (OWO), Yoon and Kim (YK), and indirect UV detection (IUV)

| Sample      | NE   | OWO   | YK   | IUV                |  |
|-------------|--|---|--|--------------------|--|
|             | $z_{\text{eff}}^{5 \text{ mM}}$<br>(Eq. 4) | $z_{\text{eff}}^{5 \text{ mM}}$<br>(Eqs. 5–7) | $z_{\text{eff}}^{5 \text{ mM}}$<br>(Eq. 8) | $z_1^a$<br>(Eq. 9) | $z_{\text{eff}}^{5 \text{ mM } a}$<br>(Eq. 14) |
| pGlu 50     | 11   | 20  | 21   | 0.38               | 19   |
| pGlu 220    | 21   | 63  | 60   | 0.39               | 85   |
| pGVE 50-20  | 16   | 39  | 37   | 0.11               | 33   |
| pGVE 100-20 | 14   | 33  | 32   | 0.11               | 35   |

<sup>a</sup> Determined by IUV method using effective mobilities ( $\mu_S$  as mentioned in Table 1,  $\mu_A=27.53 \cdot 10^{-9} \text{ m}^2 \text{ s}^{-1} \text{ V}^{-1}$  and  $\mu_C=2.36 \cdot 10^{-9} \text{ m}^2 \text{ s}^{-1} \text{ V}^{-1}$ )

used to calculate  $\alpha_S$ ), the IUV method leads to the effective charge number per non-modified glutamate ( $z_1$ ), and values are gathered in Table 2.

The comparison of  $z_1$  values obtained for the different samples allows studying the influence of the presence of VE in the chain on the polymer effective charge. For pGlu 50 and pGlu 220 (polyelectrolytes without VE), a  $z_1$  value of  $\sim 0.4$  is close to the predicted value expected by the Manning theory (0.5). This slightly lower experimental value can be explained by the incomplete dissociation of pGlu at pH 7.4 especially at low ionic strength [70]. A decrease in  $z_1$  values with the presence of VE was observed ( $z_1 \sim 0.1$  for 20 % VE). This effect can be due to the influence of the hydrophobic VE groups on the dissociation of glutamate groups. Indeed, it is known that a  $pK_a$  shift toward a higher value is observed for the carboxylic group at the vicinity of a hydrophobic domain of low dielectric constant, decreasing the dissociation degree [71].

Since the validity of the IUV method is not dependent on the nature of the solutes, the previous results are considered as the values of reference and were compared to those derived from electrophoretic mobility modeling. The NE, OWO, and YK models are based on the electrophoretic mobility of the nanogel entity. Therefore, these models lead to the effective charge number per nanogel ( $z_{\text{eff}}$ ) determined by Eq. 4 (NE), Eqs. 5–7 (OWO), and Eq. 8 (YK), respectively. It should be mentioned that at the working ionic strength of 5 mM, the conditions of validity of both OWO ( $\zeta < 100 \text{ mV}$ ) and YK ( $\kappa R_h < 25$  and  $\zeta < 200 \text{ mV}$ ) are fulfilled. The comparison between  $z_{\text{eff}}$  and  $z_1$  is possible if one considers the number  $N$  of polymer chain per hydrogel entity according to the following equation:

$$z_{\text{eff}} = z_1 N f DP \quad (14)$$

where  $N$  is the number of polymer chains per hydrogel unit. These  $N$  values were derived from static light scattering experiments conducted on dilute polymer solutions ( $1 \text{ g L}^{-1}$ ) in NaCl 150 mM. There is no influence of the

ionic strength on  $N$  for these nanogels containing 20 % of VE.

Applying NE using  $\mu_{\text{ep}}^{\infty}$  is not possible because there is no experimental method or theoretical model allowing the extrapolation of the electrophoretic mobility at infinite dilution for this kind of solute [48]. Note that the extrapolation of the hydrodynamic radius to infinite dilution would also be challenging. As a consequence, the NE relationship was applied using  $\mu_{\text{ep}}$  determined at 5 mM ionic strength in 50 mM BisTris/5 mM *p*-anisic acid buffer.  $z_{\text{eff}}$  results are gathered in Table 2. OWO and YK modelings give similar results, while NE strongly underestimates  $z_{\text{eff}}$ . This bias was expected since the electrophoretic retardation and relaxation effects cannot be neglected at finite ionic strength [47, 48, 59]. A

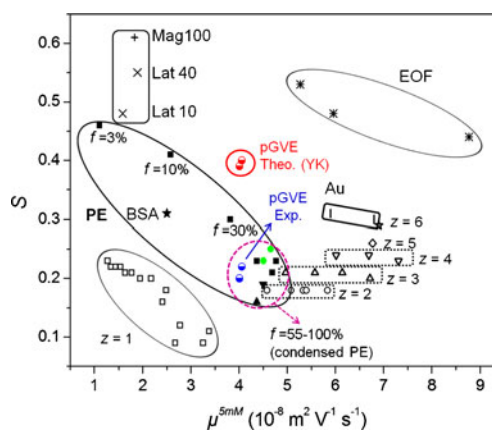


**Fig. 5** pGVE samples located on the slope plot in comparison with other samples from the literature [72].  $S$  parameter was determined experimentally using Eq. 15. Experimental values of pGVE samples are in blue. In red are represented the theoretical data that would be obtained for hard core nanoparticles having the same  $z_{\text{eff}}$  and  $R_h$  as pGVE according to the YK modeling (see “Results and discussion” section). pGlu 50 and pGlu 220 samples are depicted on the slope plot as green circles. PE zone corresponds to polyelectrolyte samples (in black).  $z=1$  to  $z=6$  zones correspond to small ions of given charge number ( $z$ ). Mag 100, Lat 10, and Lat 40 correspond to magnetic nanoparticle and nanolatexes, respectively. EOF stands for electroosmotic mobilities considered as micronic particles and BSA for bovine serum albumin as an example of proteins



consequence is that, in the conditions of the experiments, the electrophoretic frictional coefficient is higher than the hydrodynamic frictional coefficient.

When comparing YK and OWO modelings to IUUV, it appears that similar results were obtained for pGVE 50-20 and 100-20 and for pGlu 50, while a high discrepancy was observed for pGlu 220. On the whole, it appears that the IUUV method was the most adapted approach allowing the comparison between these samples since it gives directly  $z_1$  values. Moreover, the IUUV detection seems to be more adapted for the pGVE samples which are supposed to contain a high content of water in their core. Strictly speaking, the application of OWO and YK modelings is restricted to charged (hard core) nanoparticles.

Electrophoretic behavior of pGVE using the slope plot approach

To give a better insight onto the nature of the pGVE samples, we localized these samples onto the so-called “slope plot” (Fig. 5). The slope plot represents the relative decrease of the electrophoretic mobility per ionic strength decade ( $S$  parameter) as a function of the electrophoretic mobility at 5 mM ionic strength,  $\mu_{ep}^{5 \text{ mM}}$  [72]. The  $S$  parameter can be obtained from the slope of the plot representing  $\frac{\mu_{ep}}{\mu_{ep}^{5 \text{ mM}}}$  as a function of  $\log I$  (see Fig. 3 in ref. [72]), where  $I$  is the ionic strength in molar:

$$S = - \frac{\partial \left( \frac{\mu_{ep}}{\mu_{ep}^{5 \text{ mM}}} \right)}{\partial \log(I)} \quad (15)$$

This approach [72] allows to distinguish the samples according to their nature (small ions, polyelectrolytes, nanoparticles) and their charge. Different zones can be distinguished on the slope plot (Fig. 5): mono-charged small ions settle in the lower left corner of the plot while multi-charged ones are distributed on horizontal lines on the right part of the plot with increasing  $S$  values with charge number ( $z$ ). (Nano)particles occupy the highest part of the plot (highest  $S$  values up to 60 %), while polyelectrolytes settle in the middle part with a linear-like decrease of  $S$  with the polyelectrolyte charge density.

As shown in Fig. 5, the experimental points corresponding to pGlu and pGVE samples fall in the polyelectrolyte zone. If these samples had a hard core particle behavior, they would appear in the nanoparticle zone (on the upper side of the plot, as represented by the red symbols

calculated from the YK modeling for a nanoparticle having the same  $z_{\text{eff}}$  and  $R_h$  as the pGlu or pGVE samples). Therefore, we can conclude that the pGVE nanogels behave electrophoretically as polyelectrolytes.

## Conclusion

In this work, the size and the effective charge characterization of drug delivery systems based on pGVE copolymers have been experimentally investigated using TDA and CE. TDA was found to be well suited for the determination of the weight average  $R_h$  of the pGVE nanogels. Regarding the charge characterization, the IUUV method allowed the straightforward determination of the effective charge per glutamate residue  $z_1$ . On the contrary, the NE relationship cannot be used since it is not possible to extrapolate the effective mobility and the hydrodynamic radius to infinite dilution. Despite the fact that OWO and YK models are restricted to nanoparticles with a hard core, these models lead to effective charge per nanogel entity in good agreement with the IUUV method for pGVE samples. The IUUV method clearly demonstrates a decrease in the effective charge with the presence of VE due to a  $pK_a$  shift toward higher values. The slope plot approach, consisting in a graphical representation of the relative decrease in electrophoretic mobility per ionic strength decade as a function of the electrophoretic mobility at 5 mM, demonstrates and confirms that the pGVE nanogels do electrophoretically behave as polyelectrolytes. This is in good agreement with the high water content in the pGVE nanogels.

**Acknowledgments** H.C. gratefully acknowledges the support from the Région Languedoc-Roussillon for the fellowship “Chercheurs d’Avenir” and from the Institut Universitaire de France.

## References

1. Duncan R (2003) The dawning era of polymer therapeutics. *Nat Rev Drug Discov* 2(5):347–360
2. Duncan R, Ringsdorf H, Satchi-Fainaro R (2006) Polymer therapeutics: polymers as drugs, drug and protein conjugates and gene delivery systems: past, present and future opportunities. *Adv Polym Sci* 192:1–8. doi:10.1007/12\_037
3. Jeong B, Bae YH, Kim SW (2000) Drug release from biodegradable injectable thermosensitive hydrogel of PEG-PLGA-PEG triblock copolymers. *J Controlled Release* 63:155–163
4. Aurand ER, Lampe KJ, Bjugstad KB (2012) Defining and designing polymers and hydrogels for neural tissue engineering. *Neurosci Res* 72(3):199–213
5. Liechty WB, Kryscio DR, Slaughter BV, Peppas NA (2010) Polymers for drug delivery systems. *Annu Rev Chem Biomol Eng* 1:149–173

6. Allen TM, Cullis PR (2004) Drug delivery systems: entering the mainstream. *Science* 303(5665):1818–1822
7. Liechty WB, Peppas NA (2012) Expert opinion: responsive polymer nanoparticles in cancer therapy. *Eur J Pharm Biopharm* 80(2):241–246
8. Couvreur P, Dubernet C, Puisieux F (1995) controlled drug-delivery with nanoparticles—current possibilities and future trends. *Eur J Pharm Biopharm* 41(1):2–13
9. Brannon-Peppas L, Blanchette JO (2004) Nanoparticle and targeted systems for cancer therapy. *Adv Drug Deliv Rev* 56(11):1649–1659
10. Jewell CM, Zhang J, Fredin NJ, Lynn DM (2005) Multilayered polyelectrolyte films promote the direct and localized delivery of DNA to cells. *J Controlled Release* 106:214–223
11. Raemdonck K, Demeester J, De Smedt S (2009) Advanced nanogel engineering for drug delivery. *Soft Matter* 5(4):707–715
12. Peppas NA, Bures P, Leobandung W, Ichikawa H (2000) Hydrogels in pharmaceutical formulations. *Eur J Pharm Biopharm* 50(1):27–46
13. Lin C-C, Anseth K (2009) PEG hydrogels for the controlled release of biomolecules in regenerative medicine. *Pharm Res* 26(3):631–643
14. Fisher O, Kim T, Dietz S, Peppas N (2009) Enhanced core hydrophobicity, functionalization and cell penetration of polybasic nanomaterials. *Pharm Res* 26(1):51–60
15. Kafka AP, Kleffmann T, Rades T, McDowell A (2009) Histidine residues in the peptide D-Lys(6)-GnRH: potential for copolymerization in polymeric nanoparticles. *Mol Pharm* 6(5):1483–1491
16. Sahiner N, Ilgin P (2010) Synthesis and characterization of soft polymeric nanoparticles and composites with tunable properties. *J Polym Sci Pol Chem* 48(22):5239–5246
17. Chan YP, Meyrueix R, Kravtsoff R, Nicolas F, Lundstrom K (2007) Review on Medusa (R): a polymer-based sustained release technology for protein and peptide drugs. *Expert Opin Drug Deliv* 4(4):441–451
18. Sharma U, Gleason NJ, Carbeck JD (2005) Diffusivity of solutes measured in glass capillaries using Taylor's analysis of dispersion and a commercial CE instrument. *Anal Chem* 77(3):806–813
19. Ye F, Jensen H, Larsen SW, Yaghmur A, Larsen C, Ostergaard J (2012) Measurement of drug diffusivities in pharmaceutical solvents using Taylor dispersion analysis. *J Pharm Biomed Anal* 61:176–183
20. Cottet H, Biron JP, Cipelletti L, Matmour R, Martin M (2010) Determination of individual diffusion coefficients in evolving binary mixtures by Taylor dispersion analysis: application to the monitoring of polymer reaction. *Anal Chem* 82(5):1793–1802
21. Le Saux T, Cottet H (2008) Size-based characterization by the coupling of capillary electrophoresis to Taylor dispersion analysis. *Anal Chem* 80(5):1829–1832
22. Leclercq L, Cottet H (2012) Fast characterization of polyelectrolyte complexes by inline coupling of capillary electrophoresis to Taylor dispersion analysis. *Anal Chem* 84(3):1740–1743
23. d'Orlye F, Varenne A, Gareil P (2008) Determination of nanoparticle diffusion coefficients by Taylor dispersion analysis using a capillary electrophoresis instrument. *J Chromatogr A* 1204(2):226–232
24. Cottet H, Martin M, Papillaud A, Souaid E, Collet H, Commeyras A (2007) Determination of dendrigraft poly-L-lysine diffusion coefficients by Taylor dispersion analysis. *Biomacromolecules* 8(10):3235–3243
25. Hawe A, Hulse WL, Jiskoot W, Forbes RT (2011) Taylor dispersion analysis compared to dynamic light scattering for the size analysis of therapeutic peptides and proteins and their aggregates. *Pharm Res* 28(9):2302–2310
26. Ostergaard J, Jensen H (2009) Simultaneous evaluation of ligand binding properties and protein size by electrophoresis and Taylor dispersion in capillaries. *Anal Chem* 81(20):8644–8648
27. Hulse WL, Forbes RT (2011) A nanolitre method to determine the hydrodynamic radius of proteins and small molecules by Taylor dispersion analysis. *Int J Pharm* 411(1–2):64–68
28. Hulse W, Forbes R (2011) A Taylor dispersion analysis method for the sizing of therapeutic proteins and their aggregates using nanolitre sample quantities. *Int J Pharm* 416(1):394–397
29. Franzen U, Vermehren C, Jensen H, Ostergaard J (2011) Physicochemical characterization of a PEGylated liposomal drug formulation using capillary electrophoresis. *Electrophoresis* 32(6–7):738–748
30. Bello MS, Rezzonico R, Righetti PG (1994) Use of Taylor-Aris dispersion for measurement of a solute diffusion-coefficient in thin capillaries. *Science* 266(5186):773–776
31. Cottet H, Biron JP, Martin M (2007) Taylor dispersion analysis of mixtures. *Anal Chem* 79(23):9066–9073
32. Gitlin I, Carbeck JD, Whitesides GM (2006) Why are proteins charged? Networks of charge-charge interactions in proteins measured by charge ladders and capillary electrophoresis. *Angew Chem Int Ed* 45(19):3022–3060
33. Seyrek E, Dubin PL, Henriksen J (2007) Nonspecific electrostatic binding characteristics of the heparin-antithrombin interaction. *Biopolymers* 86(3):249–259
34. Manning GS (1969) Limiting laws and counterion condensation in polyelectrolyte solutions. I. Colligative properties. *J Chem Phys* 51(3):924–933
35. Chepelianskii A, Mohammad-Rafiee F, Trizac E, Raphael E (2009) On the effective charge of hydrophobic polyelectrolytes. *J Phys Chem B* 113(12):3743–3749
36. Essafi W, Lafuma F, Baigl D, Williams CE (2005) Anomalous counterion condensation in salt-free hydrophobic polyelectrolyte solutions: osmotic pressure measurements. *Europhys Lett* 71(6):938–944
37. Allison SA, Perrin C, Cottet H (2011) Modeling the electrophoresis of oligolysines. *Electrophoresis* 32(20):2788–2796
38. Vuletich T, Babic SD, Grgic D, Aumiler D, Radler J, Livolant F, Tomic S (2011) Manning free counterion fraction for a rodlike polyion: aqueous solutions of short DNA fragments in presence of very low added salt. *Physical Review E* 83(4):8–16
39. Boisvert JP, Malgat A, Pochard I, Daneault C (2002) Influence of the counter-ion on the effective charge of polyacrylic acid in dilute condition. *Polymer* 43(1):141–148
40. Combet J, Rawiso M, Rochas C, Hoffmann S, Boue F (2011) Structure of polyelectrolytes with mixed monovalent and divalent counterions: SAXS measurements and Poisson–Boltzmann analysis. *Macromolecules* 44(8):3039–3052
41. Bohme U, Scheler U (2003) Effective charge of poly(styrenesulfonate) and ionic strength—an electrophoresis NMR investigation. *Colloids Surf A* 222(1–3):35–40
42. Anik N, Airiau M, Labeau MP, Vuong CT, Reboul J, Lacroix-Desmazes P, Gerardin C, Cottet H (2009) Determination of polymer effective charge by indirect UV detection in capillary electrophoresis: toward the characterization of macromolecular architectures. *Macromolecules* 42(7):2767–2774
43. Pyell U, Bucking W, Huhn C, Herrmann B, Merkoulov A, Mannhardt J, Jungclas H, Nann T (2009) Calibration-free concentration determination of charged colloidal nanoparticles and determination of effective charges by capillary isotachopheresis. *Anal Bioanal Chem* 395(6):1681–1691
44. Agnihotri SM, Ohshima H, Terada H, Tomoda K, Makino K (2009) Electrophoretic mobility of colloidal gold particles in electrolyte solutions. *Langmuir* 25(8):4804–4807

45. Oukacine F, Morel A, Cottet H (2011) Characterization of carboxylated nanolatexes by capillary electrophoresis. *Langmuir* 27(7):4040–4047
46. Xin Y, Mitchell H, Cameron H, Allison SA (2006) Modeling the electrophoretic mobility and diffusion of weakly charged peptides. *J Phys Chem B* 110(2):1038–1045
47. Li SK, Liddell MR, Wen H (2011) Effective electrophoretic mobilities and charges of anti-VEGF proteins determined by capillary zone electrophoresis. *J Pharm Biomed Anal* 55(3):603–607
48. Ibrahim A, Ohshima H, Allison SA, Cottet H (2012) Determination of effective charge of small ions, polyelectrolytes and nanoparticles by capillary electrophoresis. *J Chromatogr A* 1247:154–164
49. Taylor G (1953) Dispersion of soluble matter in solvent flowing slowly through a tube. *Proc R Soc London, Ser A* 219(1137):186–203
50. Aris R (1956) On the dispersion of a solute in a fluid flowing through a tube. *Proc R Soc London, Ser A* 235(1200):67–77
51. Chamieh J, Oukacine F, Cottet H (2012) Taylor dispersion analysis with two detection points on a commercial capillary electrophoresis apparatus. *J Chromatogr A* 1235:174–177
52. Taylor G (1954) Conditions under which dispersion of a solute in a stream of solvent can be used to measure molecular diffusion. *Proc R Soc London, Ser A* 225(1163):473–477
53. Chamieh J, Cottet H (2012) Comparison of single and double detection points Taylor dispersion analysis for monodisperse and polydisperse samples. *J Chromatogr A* 1241:123–127
54. Einstein A (1906) A new determination of the molecular dimensions. *Ann Phys* 19(2):289–306
55. Stokes G (1966) Vol Cambridge Philos Trans 1851;9:8. Reprinted in: *Mathematical and Physical Papers*, 2nd edition. Johnson Reprint Corp., New York
56. Pitts E (1953) An extension of the theory of the conductivity and viscosity of electrolyte solutions. *Proc R Soc London, Ser A* 217(1128):43–70
57. Plasson R, Cottet H (2005) Determination of homopolypeptide conformational changes by the modeling of electrophoretic mobilities. *Anal Chem* 77(18):6047–6054
58. Friedl W, Reijenga JC, Kenndler E (1995) Ionic-strength and charge number correction for mobilities of multivalent organic-anions in capillary electrophoresis. *J Chromatogr A* 709(1):163–170
59. Long D et al (1996) A Zimm model for polyelectrolytes in an electric field. *J Phys Condens Matter* 8(47):9471–9475
60. Ohshima H (2001) Approximate analytic expression for the electrophoretic mobility of a spherical colloidal particle. *J Colloid Interface Sci* 239(2):587–590
61. Makino K, Ohshima H (2010) Electrophoretic mobility of a colloidal particle with constant surface charge density. *Langmuir* 26(23):18016–18019
62. Yoon BJ, Kim S (1989) Electrophoresis of spheroidal particles. *J Colloid Interface Sci* 128(1):275–288
63. Allison SA, Pei HX, Baek S, Brown J, Lee MY, Nguyen V, Twahir UT, Wu HF (2010) The dependence of the electrophoretic mobility of small organic ions on ionic strength and complex formation. *Electrophoresis* 31(5):920–932
64. Ohshima H (1994) A simple expression for henrys function for the retardation effect in electrophoresis of spherical colloidal particles. *J Colloid Interface Sci* 168(1):269–271
65. O'Brien RW, White LR (1978) Electrophoretic mobility of a spherical colloidal particle. *J Chem Soc Faraday Trans 2*(74):1607–1626
66. Doble P, Andersson P, Haddad PR (1997) Determination and prediction of transfer ratios for anions in capillary zone electrophoresis with indirect UV detection. *J Chromatogr A* 770(1–2):291–300
67. Hjerten S, Elenbring K, Kilar F, Liao JL, Chen AJC, Siebert CJ, Zhu MD (1987) Carrier-free zone electrophoresis, displacement electrophoresis and isoelectric-focusing in a high-performance electrophoresis apparatus. *J Chromatogr* 403:47–61
68. Johns C, Macka M, Haddad PR (2003) Enhancement of detection sensitivity for indirect photometric detection of anions and cations in capillary electrophoresis. *Electrophoresis* 24(12–13):2150–2167
69. Kohlrausch F (1897) Ueber Concentrations-Verschiebungen durch Electrolyse im Inneren von Lösungen und Lösungsgemischen. *Ann Phys* 298(10):209–239
70. Nishio T (1998) Monte Carlo studies on potentiometric titration of poly(glutamic acid). *Biophys Chem* 71(2–3):173–184
71. Holm C, Joanny JF, Kremer K, Netz RR, Reineker P, Seidel C, Vilgis TA, Winkler RG (2004) Polyelectrolyte theory. In: Schmidt M (ed) *Polyelectrolytes with defined molecular architecture*. Springer, Berlin, pp 67–111
72. Ibrahim A, Allison SA, Cottet H (2012) Extracting information from the ionic strength dependence of electrophoretic mobility by use of the slope plot. *Anal Chem* 84:9422–9430